Supporting Information

Visualizing chiral structures in cellulose nanocrystal films by Mueller matrix

Xiaowei Feng‡[a], Ting Wang‡[b], Mengyuan Hao[a], Nichang Xue[a], Haidan Zhu[a], Yang Tian*[a] and Xiaoyan Cui*[a]

[a] School of Chemistry and Molecular Engineering, East China Normal University, 500 Dongchuan Road, Shanghai, 200241, (P.R. China).

[b] College of Pharmacy, Naval Medical University, 800 Xiangyin Road, Shanghai, 200433, (P.R. China).

*e-mail: ytian@chem.ecnu.edu.cn; xycui@chem.ecnu.edu.cn;

‡Both authors contributed equally to the work.

Table of Content

1. Materials and Characterizations

Materials

All reagents were purchased from commercial suppliers and used without further purification. CNCs used in this work were purchased from ScienceK Co. Ltd, Zhejiang, China. Congo red (CR, CI# 22120) was purchased from TCI, Methylene blue (MB, CI# 52015), Trypan blue (TB, CI# 23850), and Chicago sky blue 6B (CSB, CI# 24410), sodium hydroxide, sulfuric acid, and sodium chloride were purchased from Shanghai Titan Scientific Co. Ltd. All reagents were of analytical grade and used without further purification.

Characterizations

Scanning electron microscopy (SEM) was performed on the Hitachi S-4800. Before evaluation, the samples were prepared and sputter-coated with gold (5.0 nm). Structures of cross-section samples were obtained by breaking films into small pieces. Atomic force microscope (AFM) was performed on a Bruker Bio-FastScan AFM in the contact mode. Polarized optical microscopy (POM) photographs were taken with a Leica DM 750P polarized microscope equipped with a Nikon D800 camera and crossed polarizers. Absorption spectra were performed on the PerkinElmer Lambda 950. CD spectra were performed in transmission mode using a JASCO J-1500 spectropolarimeter by rotating the sample from 0° to 360° at 45° intervals. Mueller matrix microscopy (MMM) images were obtained using a home-built Mueller matrix polarimeter (Figure S1). The design principle was described previously.[1-5] In short, it is customized with polarization state modulators based on dual rotating wave plates. By rotating a pair of quarter-wave plates, which is respect to two stationary linear polarizers, the time-averaged polarization states of light before and after the propagation of the sample can be obtained and then were demodulated to recover M. All the data are displayed as a 4×4 array of pseudo-color images each representing one element of the M matrix.

2. Experimental Methods

2.1 Preparation of CNCs aqueous suspensions

Aqueous suspensions of CNCs (6.0 wt.%, pH 6.0-7.0) were prepared using an ultrasonic bio-mixer 600 W ultrasonic processor installed in a 6-mm-diameter probe. Typically, 0.51 g CNCs in 8.0 g deionized water were mixed in a 50 mL centrifuge tube and sonicated at 60 W for 40 min in an ice bath to prevent de-sulfation.

2.2 Preparation of aqueous solution for dye molecules

Different dyes were dissolved in distilled water to prepare aqueous solutions with a concentration of 5.0 mM.

2.3 Fabrication of chromophore-aligned CNC films

An effective way to achieve chiral signal amplification is to use the specific physical interaction between CNCs and chromophores. In this case, the highly aligned transition electric dipole moments of dye molecules contribute to the increased intensity of |LD|, while the CD arises accordingly. Thus, the |LD| and CD increased dramatically in the absorption region of dye than in the non-absorption region while maintaining the intensity of LB and CB. In a typical procedure, 30 μL solution of dye molecules aqueous solution was added to 2.0 g deionized water and stirred for 30 min for a homogenous solution, then 1.0 g CNC aqueous suspension (6.0 wt.%) was added. Next, the mixture was magnetically stirred for 1 h at room temperature and sonicated for 5 min, generating a homogeneous suspension. Finally, drops of the mixed suspension were cast on a clean glass slide and dried at controlled temperature and humidity (6 ˚C, 67% relative humidity (R.H.)).

2.4 Fabrication of CNC films with different NaCl concentrations

50 μM dye molecules aqueous solution was added into the NaCl solution with different concentrations (0 mM, 0.20 mM, 0.50 mM, 0.75 mM, 1.0 mM, 1.3 mM and 1.5 mM) and stirred for 30 min, then 1.0 g CNC suspension (6.0 wt.%) was added. The mixture was magnetically stirred for 1 h at room temperature and sonicated for 5 min to generate a homogeneous suspension. Drops of the mixed suspension were cast on a slide and dried at controlled temperature and humidity (6 ˚C, 67% R.H.).

2.5 Fabrication of CNC films with different pH values

1.0 g CNCs suspension (6.0 wt.%) was added to 2.0 g deionized water with 50 μM dye molecules aqueous solution, then 10 % sulfuric acid and 1.0 M sodium hydroxide were used to tune the pH to 5.1, 6.3, 7.3, 8.4, 9.5, and 10.1, respectively. The mixture was magnetically stirred for 1 h at room temperature and sonicated for 5 min, generating a homogeneous suspension. Drops of the mixed suspension were cast on a slide and dried at controlled temperature and humidity (6 ˚C, 67% R.H.).

2.6 Fabrication of CNC films with different CNCs concentrations

The original 6.0 wt.% CNC suspension was diluted with different volumes of deionized water to tune the concentrations to about 0.50 wt.%, 1.0 wt.%, 1.5 wt.%, 2.0 wt.%, and 2.5 wt.%, respectively. The concentration of dye molecules in each solution was 50 μM. The mixture was magnetically stirred for 1 h at room temperature and sonicated for 5 min, generating a homogeneous suspension. Drops of the mixed suspension were cast on a slide and dried at controlled temperature and humidity (6 ˚C, 67% R.H.).

2.7 CNC films grown at different evaporating temperatures

1.0 g CNCs suspension (6.0 wt.%) was added to 2.0 g deionized water with 50 μM dye solution. The mixture was magnetically stirred for 1 h at room temperature and sonicated for 5 min, generating a homogeneous suspension. Drops of the mixed suspension were cast on a slide and dried at 5 ˚C, 15 ˚C, 25 ˚C, 35 ˚C, and 45 ˚C respectively.

2.8 Bleach the chromophore-aligned CNC films

Samples are exposed under the laser (80 mV, 560 nm) and irradiation for 4 h with a stencil above the film.

3. Optical Model

In the defined Cartesian coordination system, the film is oriented in the *xy* plane (Figure 2), and all the Mueller matrices of the films are simulated along the *z*-axis. The CNC films are composed of the *P* layers of continuously rotated CNC nanocrystallite, whose refractive indices are n_x = 1.520, n_y =1.544, and n_z = 1.594.[6, 7] The thickness of the CNC film (*H*) and width of each CNC nanocrystalline (*d*) are measured in the SEM analysis. The helicoidal assembly of the CNC film from nanocrystallites is defined by the rotational angle between the successively twisted CNC fibers along the helical direction $\vec{m}$ (φ), the tilted angle of the helix (θ) between$\vec{m}$ and $\vec{z}$, and the periodic for different stakes of helical CNC normal to $\vec{m}$ (ω), in the defined Cartesian coordinate system with ω = 0, $n_z//\vec{y}$, $n_y//\vec{x}$, $n_x//\vec{z}$. The contribution from the aligned dye molecules in the p^{th} layer is D, which is related to the dispersion and absorption of the parallelly aligned dyes. Thus, the optical properties O of each CNC nanocrystallite are contributed by both the orientation of the refractive indices in the crystallite and aligned transition electric dipole moment from the dye molecules as follows:

$$O = \begin{bmatrix} n_y^2 & 0 & 0 \\ 0 & n_z^2 & 0 \\ 0 & 0 & n_x^2 \end{bmatrix} + D \qquad (1)$$

The orientation of the p^{th} layer is defined as a product of the rotation matrices: $R_{\vec{m}}(\psi)R_{\perp}(\omega)$. $R_{\vec{m}}(\psi)$ is a rotation matrix for rotation around the helical axis $\vec{m}$ by an angle ψ, the summed up φ in the p^{th} layer of CNC. $R_{\perp}(\omega)$ is a rotation matrix represents the rotation around the axis normal to $\vec{m}$ by an angle, ω. The electric permittivity tensor of the p^{th} layer (ε_p) is defined as $\varepsilon_p = R_{\vec{m}}(\psi)R_{\perp}(\omega)OR_{\vec{m}}^{T}(\psi)R_{\perp}^{T}(\omega)$, where T denotes the transposed matrix.

The Jones matrix of the p^{th} layer J_p is described by the incident wave-vector along the *z*-axis and written as the eigen decomposition by the eigenvalues (W) and eigenvectors (V) of the electric permittivity tensor ε_p,[8]

$$J_p = V\begin{bmatrix} e^{-ikW} & 0 \\ 0 & e^{-ikW} \end{bmatrix}V^{-1} \qquad (2)$$

where *k* is a constant in terms of CNC nanocrystalline thickness (*d*) and measuring wavelength (λ). The Jones matrix of the overall helicoidal assemble is the multiplication of the successive layers $J = \prod_{1}^{P} J_p$. The Jones matrix (J) was transferred to a Mueller matrix by its conjugate matrix (J^*) using $M = A(J \otimes J^*)A^{-1}$, where $\otimes$ indicates the Kronecker product, A is a 4×4 constant matrix defined by

$$A = \frac{\sqrt{2}}{2}\begin{bmatrix} 1 & 0 & 0 & 1 \\ 1 & 0 & 0 & -1 \\ 0 & 1 & 1 & 0 \\ 0 & i & -i & 0 \end{bmatrix} \qquad (3)$$

The optical response of the CNC films can be generated by the matrix exponential (L), which is connected to M by[9, 10]

$$M = \exp(L) = exp\begin{bmatrix} C & -LD & -LD' & CD \\ -LD & C & CB & LB' \\ -LD' & -CB & C & -LB \\ CD & -LB' & LB & C \end{bmatrix} \qquad (4)$$

where *C* corresponds to the sum of the total absorption.

4. Supplementary Figures

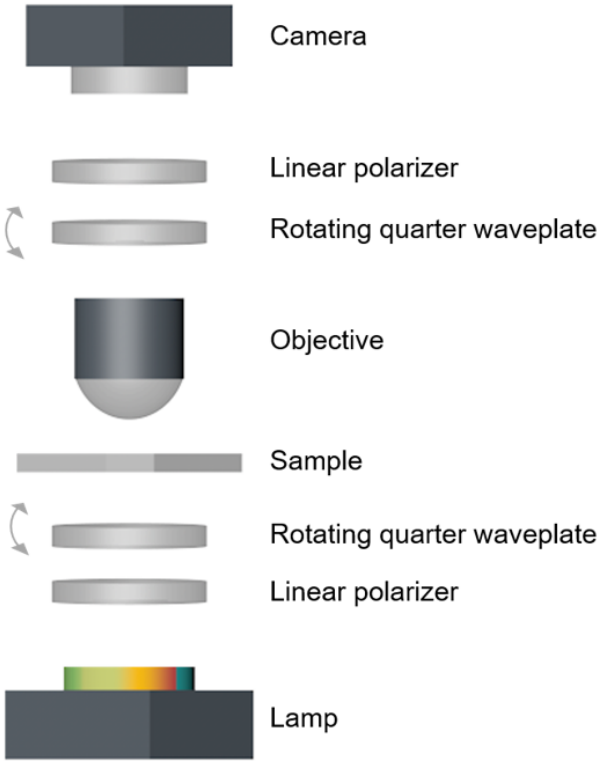

Figure S1 | Schematic structure of the Muller matrix microscope.

As a powerful imaging technique for structural analysis, MMM can completely image the optical properties of the crystalline structures.[4, 11] In MMM, the polarization properties of the sample are analyzed by monitoring the time-averaged polarization states of light before and after the propagation of the sample, using the four-elements Stokes vector, S.[12] Thus, it can be written as $S_{out} = MS_{in}$, where M represents the 4×4 Mueller matrix that contains the full optical properties of the sample, including CD, circular birefringence (CB), linear birefringence (LB), linear dichroism (LD), and the respective orientations of LB and LD.[13] For the non-depolarizing M that has an unchanged degree of polarization, the 16 elements can be reduced into seven by matrix exponential through M = exp L, in which the elements are directly associated with the LB, LB', LD, LD', CB, CD, and the total absorption of sample (*C*).[11] Here, M is composed of 16 images through capturing the intensity of light with the camera in the home-built MMM. All the optical properties are represented by their pseudo-color maps. LB and LB' are the angular distribution related by $|LB| = \sqrt{LB^2 + LB'^2}$ and the orientation of LB is $2LB_{angle} = atan2(LB', LB)$. Similarly, $|LD| = \sqrt{LD^2 + LD'^2}$ and $2LD_{angle} = atan2(LD', LD)$.[14]

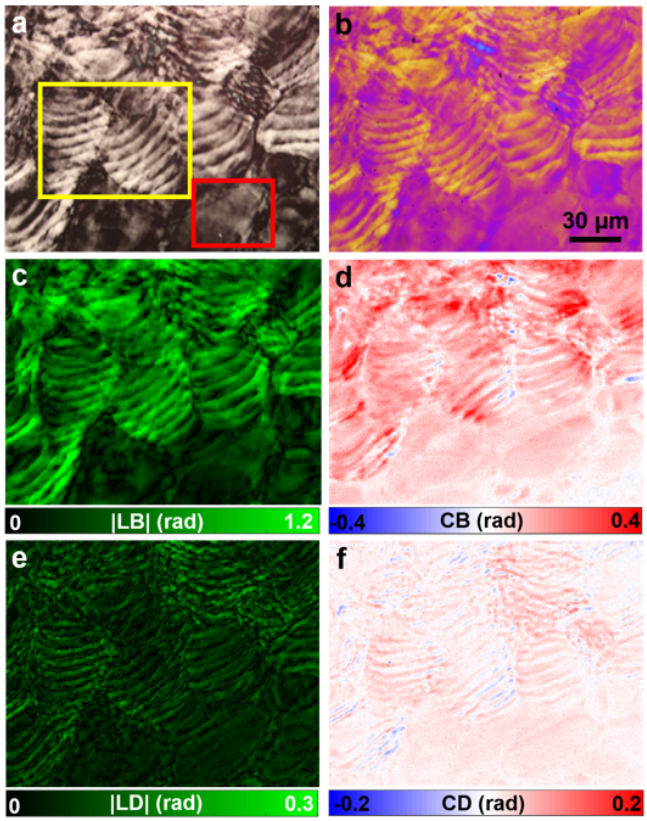

Figure S2. Optical properties of the CNC film with different domains. (a) POM observed under crossed polarizers (fingerprint regions in the yellow square and planar regions in the red square), and (b) with 530 nm full-wave retardation plate inserted. (c-f) corresponding pseudo-color maps for optical properties by MMM, including (c) |LB|, (d) CB, (e) |LD|, and (f) CD.

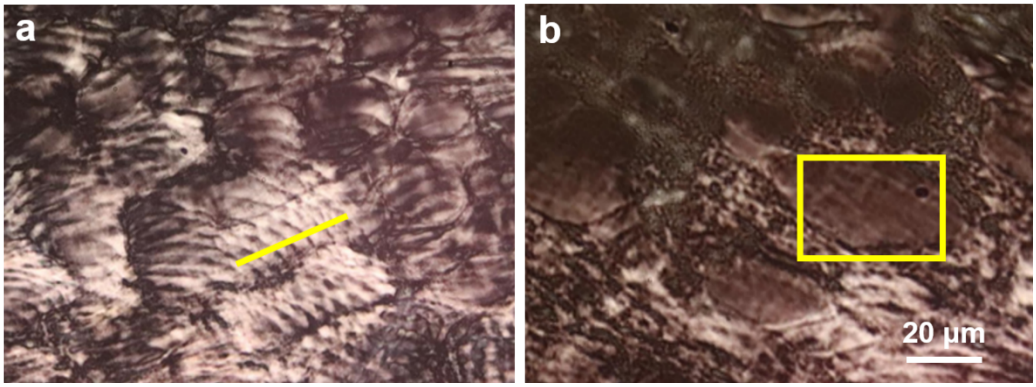

Figure S3 | POM images of the microdomains shown in Figure 1a and 1b.

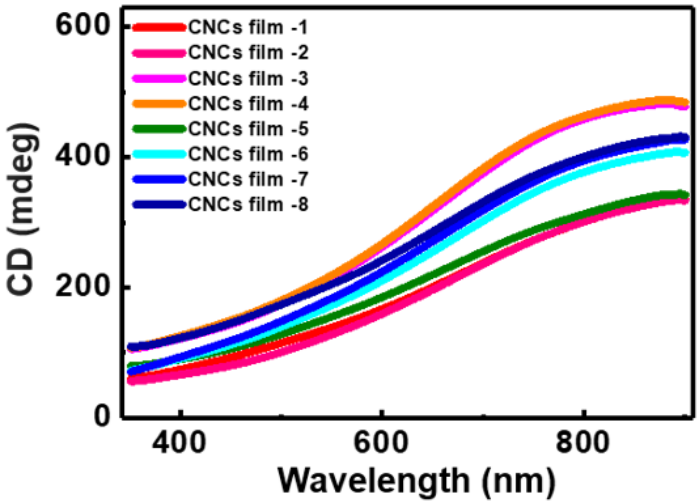

Figure S4 | Circular dichroism (CD) spectra of the CNC film with eight different orientations, respectively.

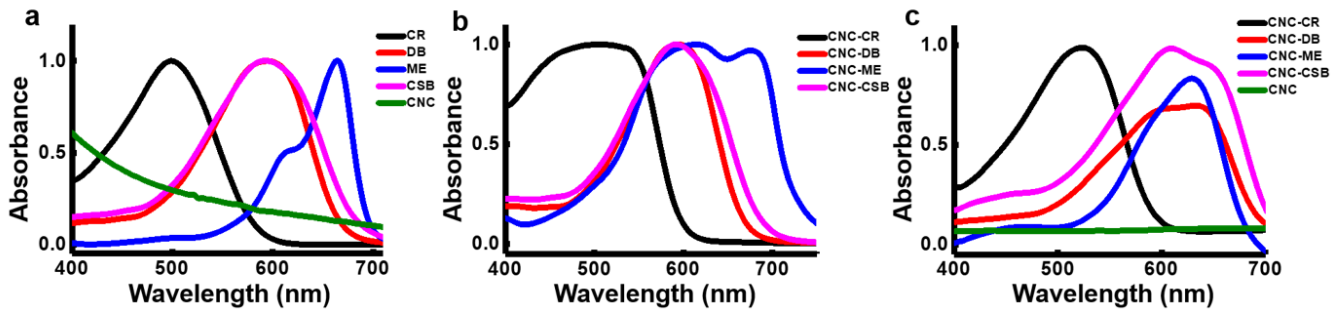

Figure S5 | Absorption spectra of (a) dye solutions and CNCs suspension, (b) CNCs suspensions contain trace amount of chromophore, and (c) the chromophore-aligned CNC films.

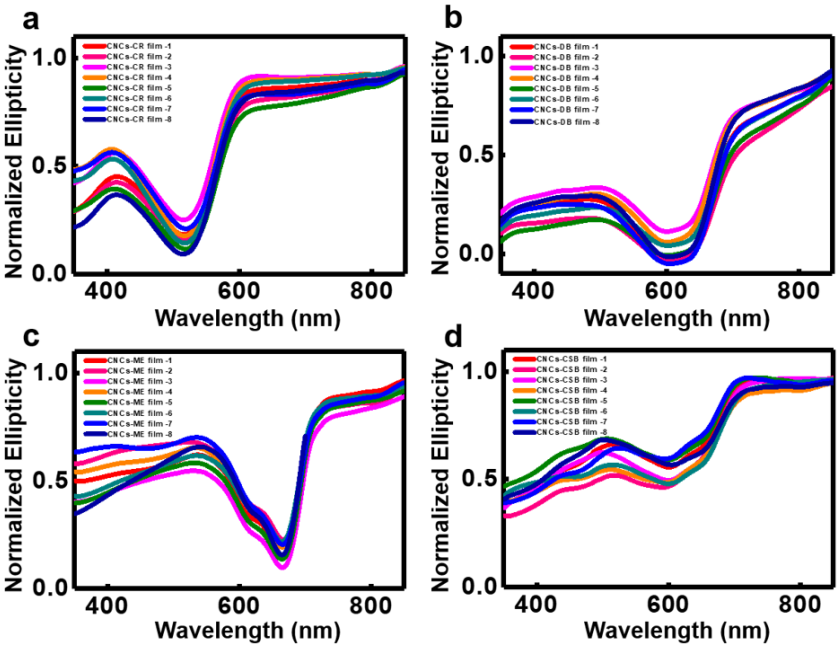

Figure S6 | The CD spectra of the (a) CNC-CR film, (b) CNC-TB film, (c) CNC-ME film, and (d) CNC-CSB film with eight different orientations, respectively.

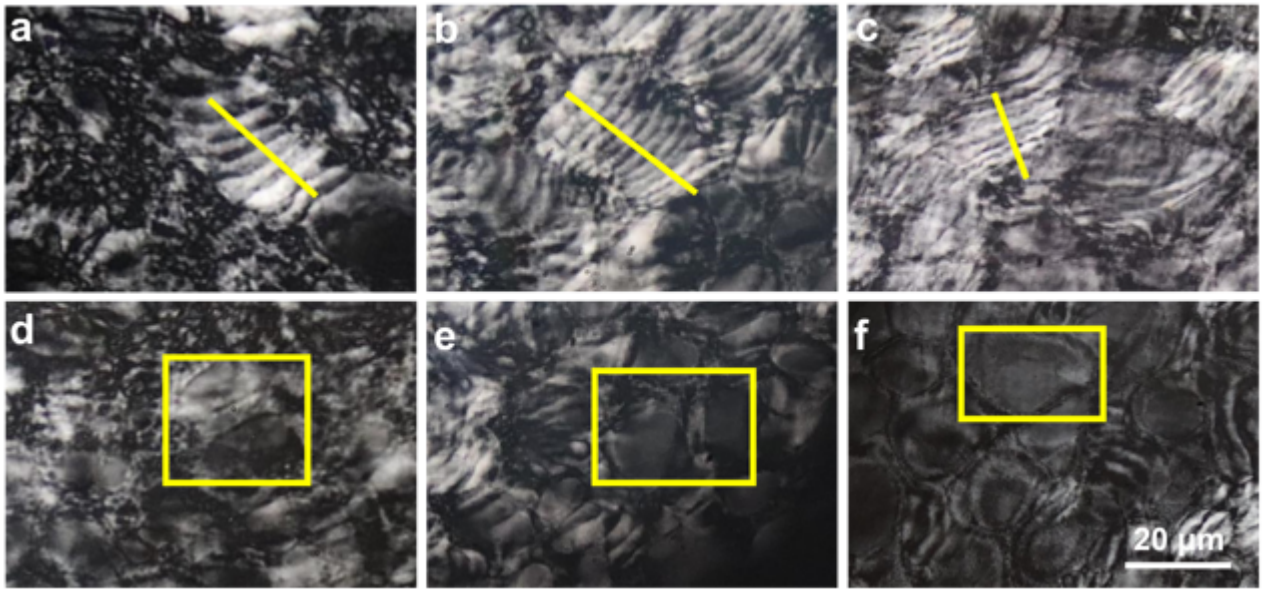

Figure S7 | POM images of the corresponding microdomains shown in Figures S8–S13.

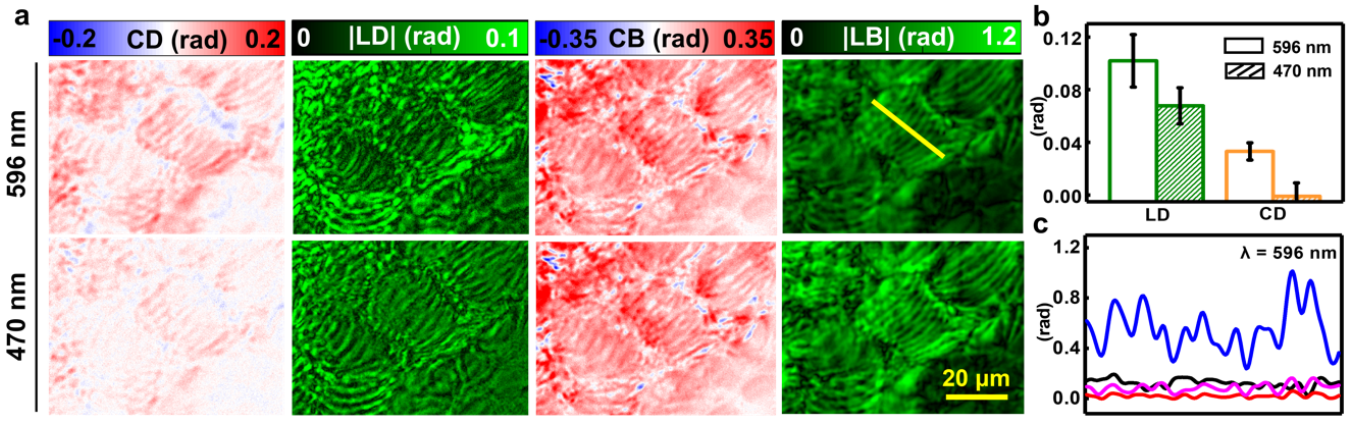

Figure S8 | MMM results of the fingerprint region in the TB dyed CNC film. (a) Measured CD, |LD|, CB, and |LB| images under 596 and 470 nm, respectively. (b) The average intensity of the |LD| and CD under 596 nm and 470 nm along the yellow lines in the |LB| images. (c) The extracted optical properties along the yellow lines in the |LB| image.

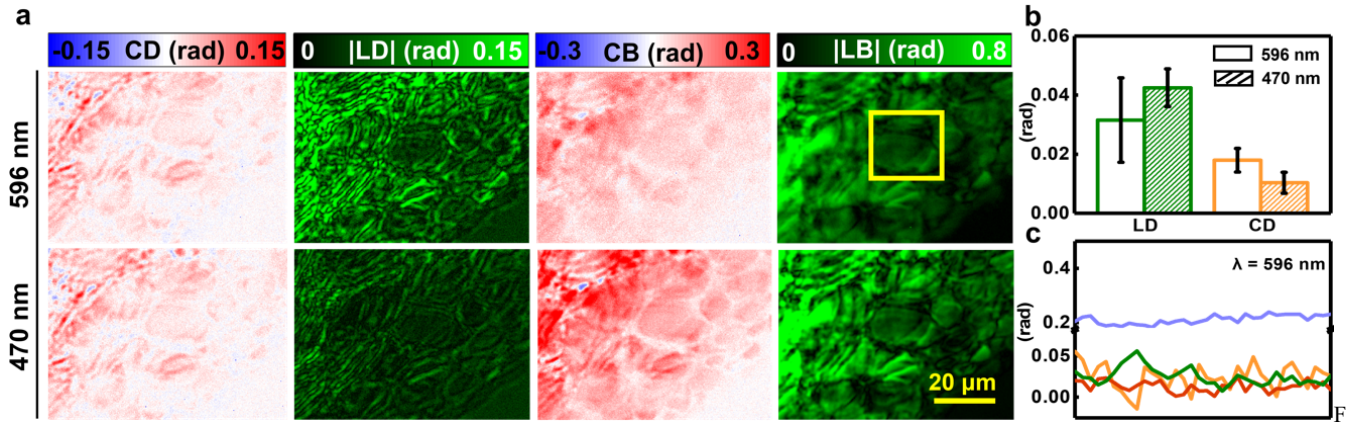

Figure S9 | MMM results of the planar region in the TB dyed CNC film. (a) Measured CD, |LD|, CB, and |LB| images under 596 and 470 nm, respectively. (b) The average intensity of the |LD| and CD under 596 nm and 470 nm in the yellow square in the |LB| image. (c) The extracted optical properties in the yellow square in the |LB| image.

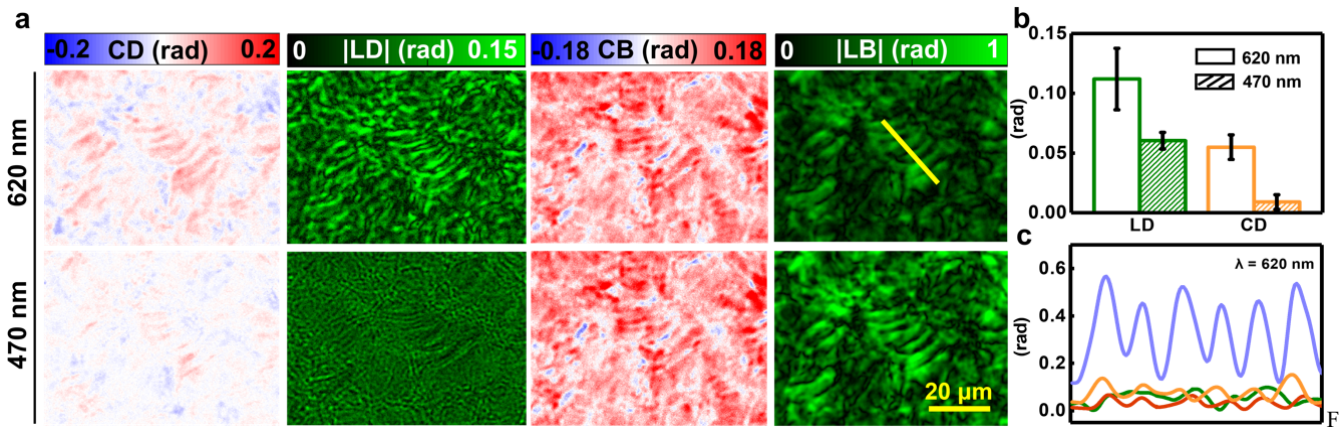

igure S10 | MMM results of the fingerprint region in the ME dyed CNC film. (a) Measured CD, |LD|, CB, and |LB| images under 620 and 470 nm, respectively. (b) The average intensity of the |LD| and CD under 620 nm and 470 nm along the yellow line in the |LB| image. (c) The extracted optical properties along the yellow line in the |LB| image.

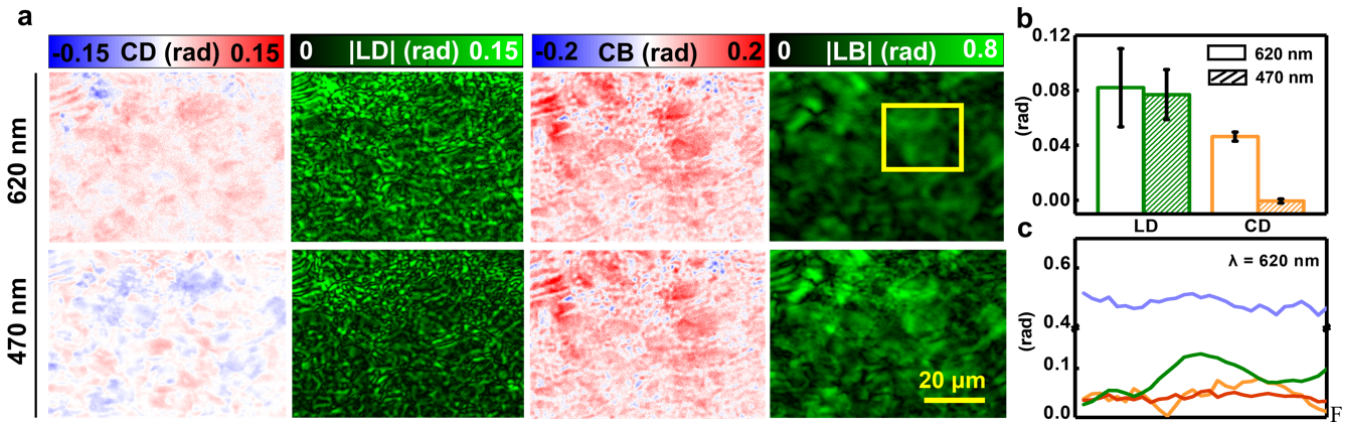

igure S11 | MMM results of the planar region in the ME dyed CNC film. (a) Measured CD, |LD|, CB, and |LB| images under 620 and 470 nm, respectively. (b) The average intensity of the |LD| and CD under620 nm and 470 nm in the yellow square in the |LB| image. (c) The extracted optical properties in the yellow square in the |LB| image.

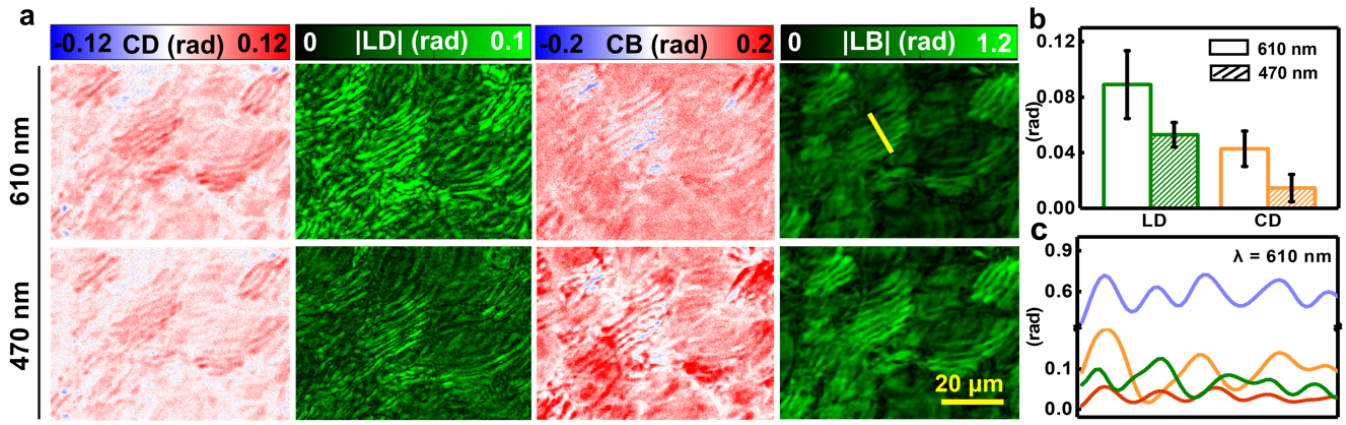

Figure S12 | MMM results of the fingerprint region in the CSB dyed CNC film. (a) Measured CD, |LD|, CB, and |LB| images under 610 and 470 nm, respectively. (b) The average intensity of the |LD| and CD under 610 nm and 470 nm along the yellow line in the |LB| image. (c) The extracted optical properties along the yellow line in the |LB| image.

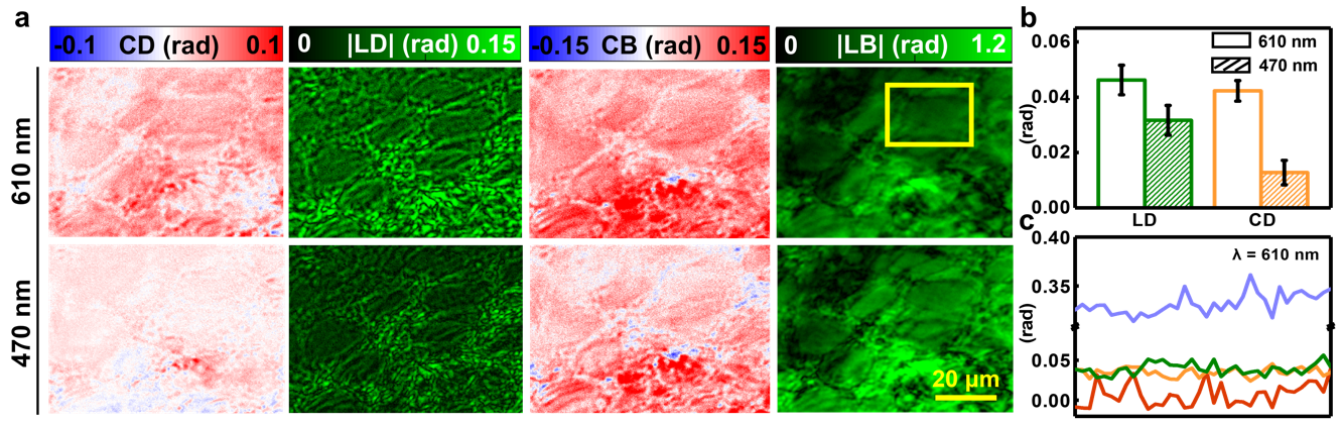

Figure S13 | MMM results of the planar region in the CSB dyed CNC film. (a) Measured CD, |LD|, CB, and |LB| images under 610 and 470 nm, respectively. (b) The average intensity of the |LD| and CD under 610 nm and 470 nm in the yellow square in the |LB| image. (c) The extracted optical properties in the yellow square in the |LB| image.

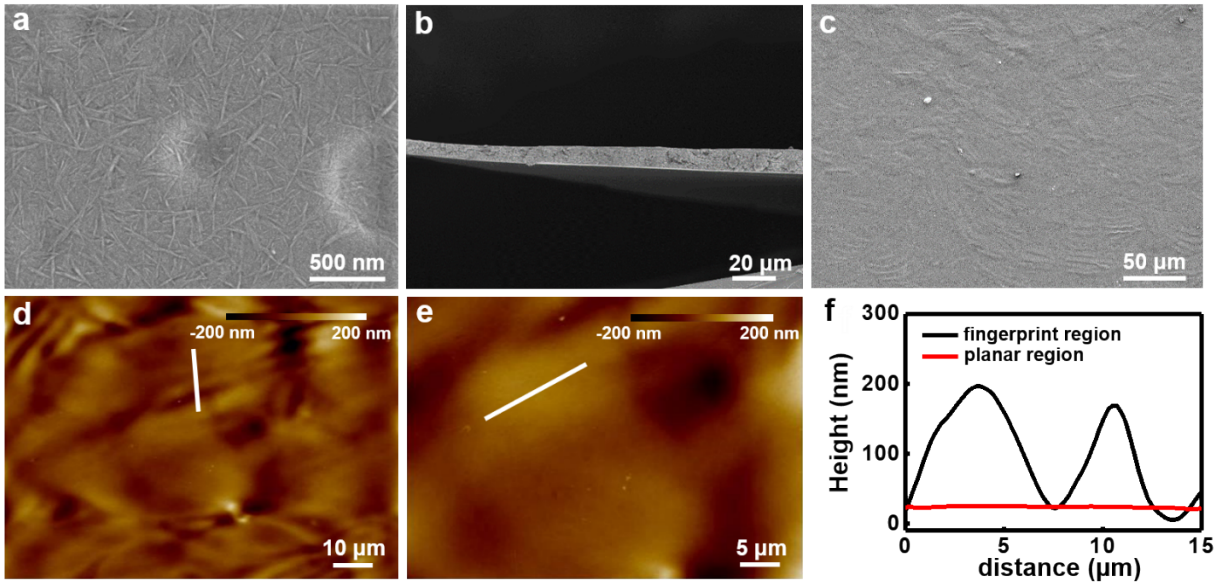

Figure S14 | (a) SEM image of CNCs. (b, c) Cross section and surface SEM images of the CNC film. (d, e) AFM images of the fingerprint and planar region in the CNC film. (f) The extracted height difference along the white lines in d and e.

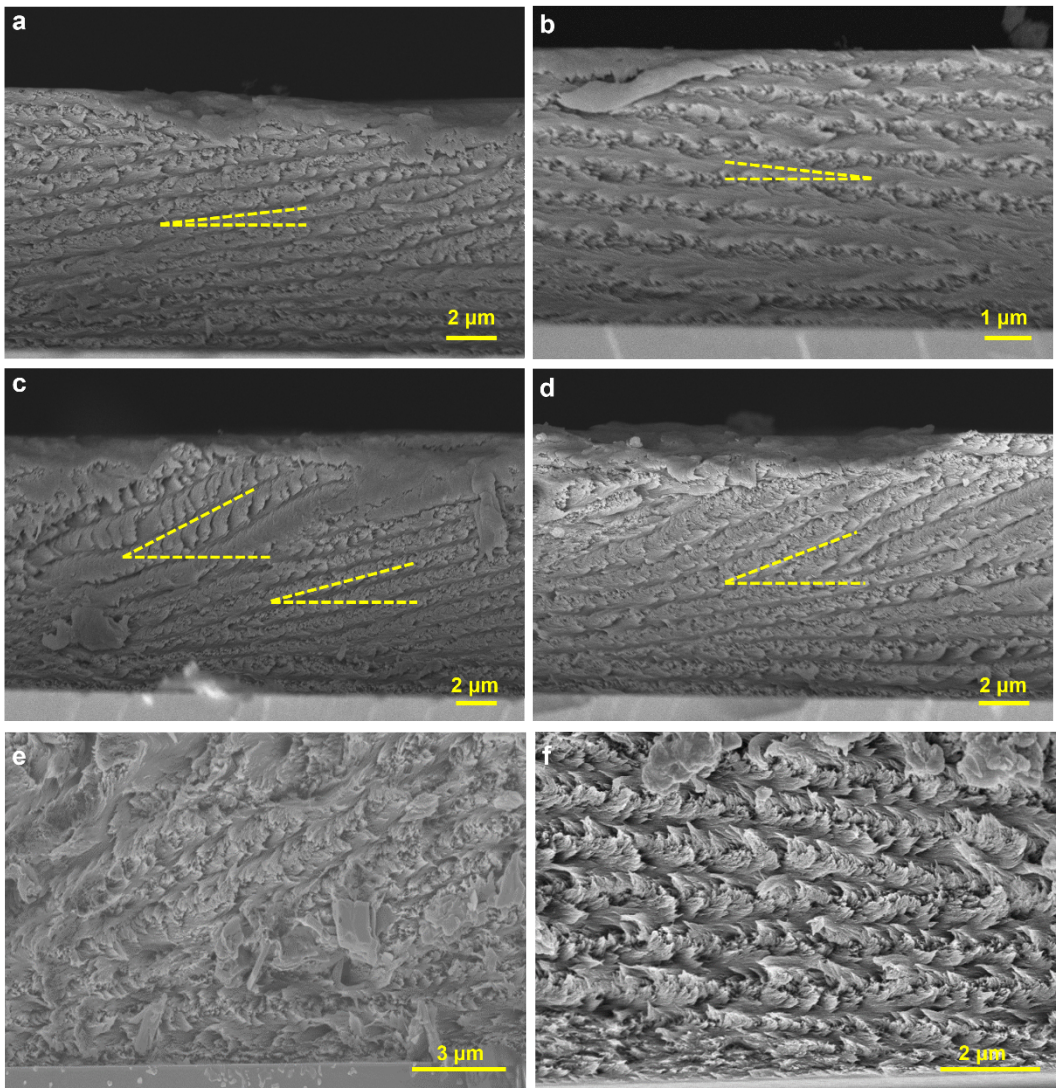

Figure S15 | Cross-sectional SEM images of the (a, b) planar and (c, d) fingerprint regions in the CNC film, and (e, f) the low magnification of Figure 1c and 1f.

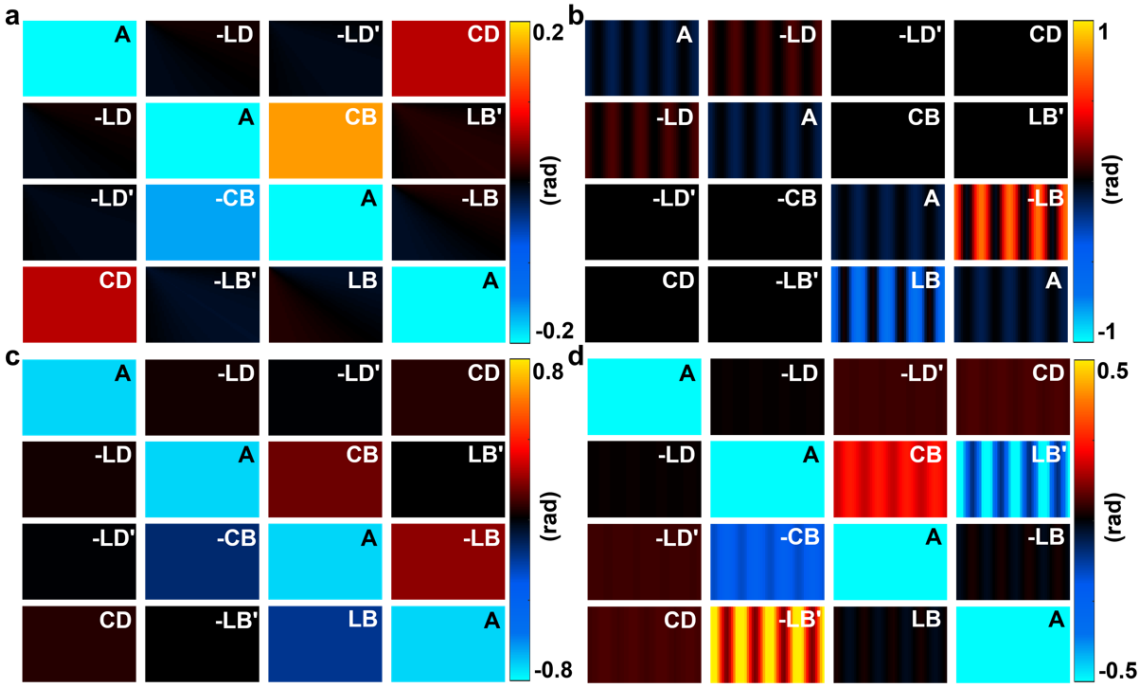

Figure S16 | The calculated optical properties of the CNC films with (a) vertical helical arrangement, (b) horizontal helical arrangement, (c) tilted helical arrangement with $\omega = 0^{\circ}$ and (d) tilted helical arrangement with $\omega = [0^{\circ}, 180^{\circ}]$.

Table S1. Experimental and simulated optical properties of CNC film.

		CB[a]	CD[a]	LB[a]	LD[a]
I[b]	Experiment[c]	0.14±0.02	0.032±0.03	0.20±0.04	0.063±0.04
	Simulation[d]	0.15	0.056	0.19	0.025
II[b]	Experiment[c]	0.12±0.03	0.050±0.002	0.74±0.20	0.076±0.01
	Simulation[d]	0.24	0.066	0.62	0.051

[a)] All the parameters are in radians. [b)] Region I represents the planar region and region II stands for the fingerprint region. [c)] The experimental results were collected from corresponding regions in Figure 1. [d)] The parameters for simulation are provided in the experimental section.

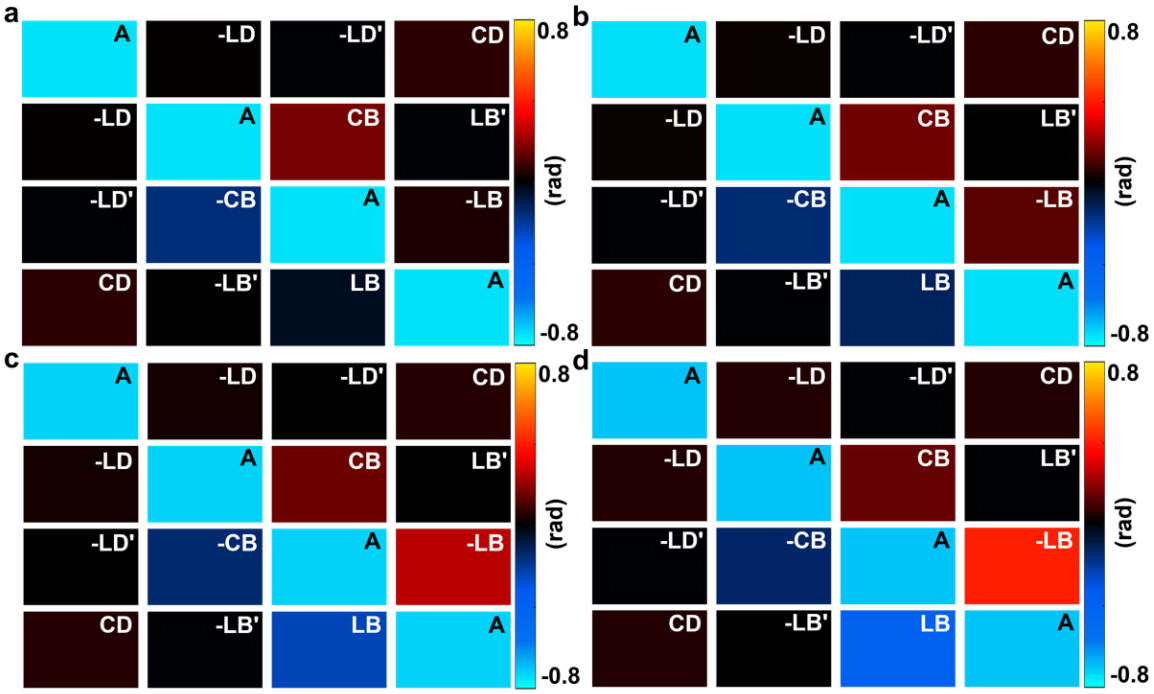

Figure S17 | The calculated optical properties of the tilted helicoidal structures with different tilted angles. a-d) $\theta = 5^{\circ}$, 10°, 15°, and 20°, respectively.

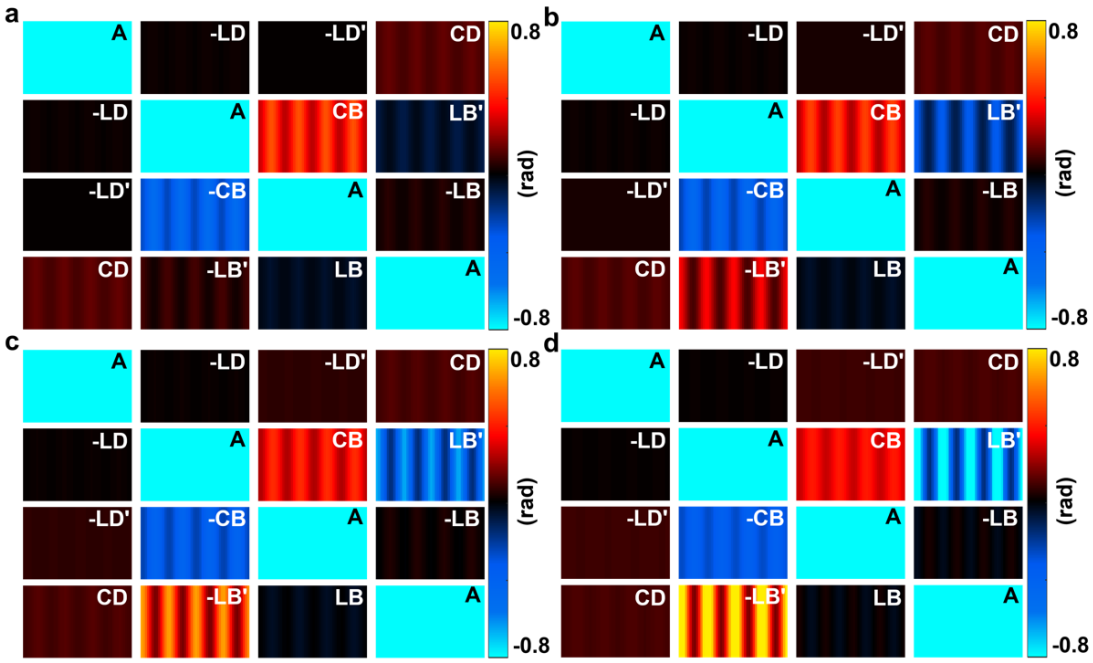

Figure S18 | The calculated optical properties of the tilted and misaligned helicoidal structure with different tilted angles. a-d) θ = 5˚, 10˚, 15˚, and 20˚, respectively.

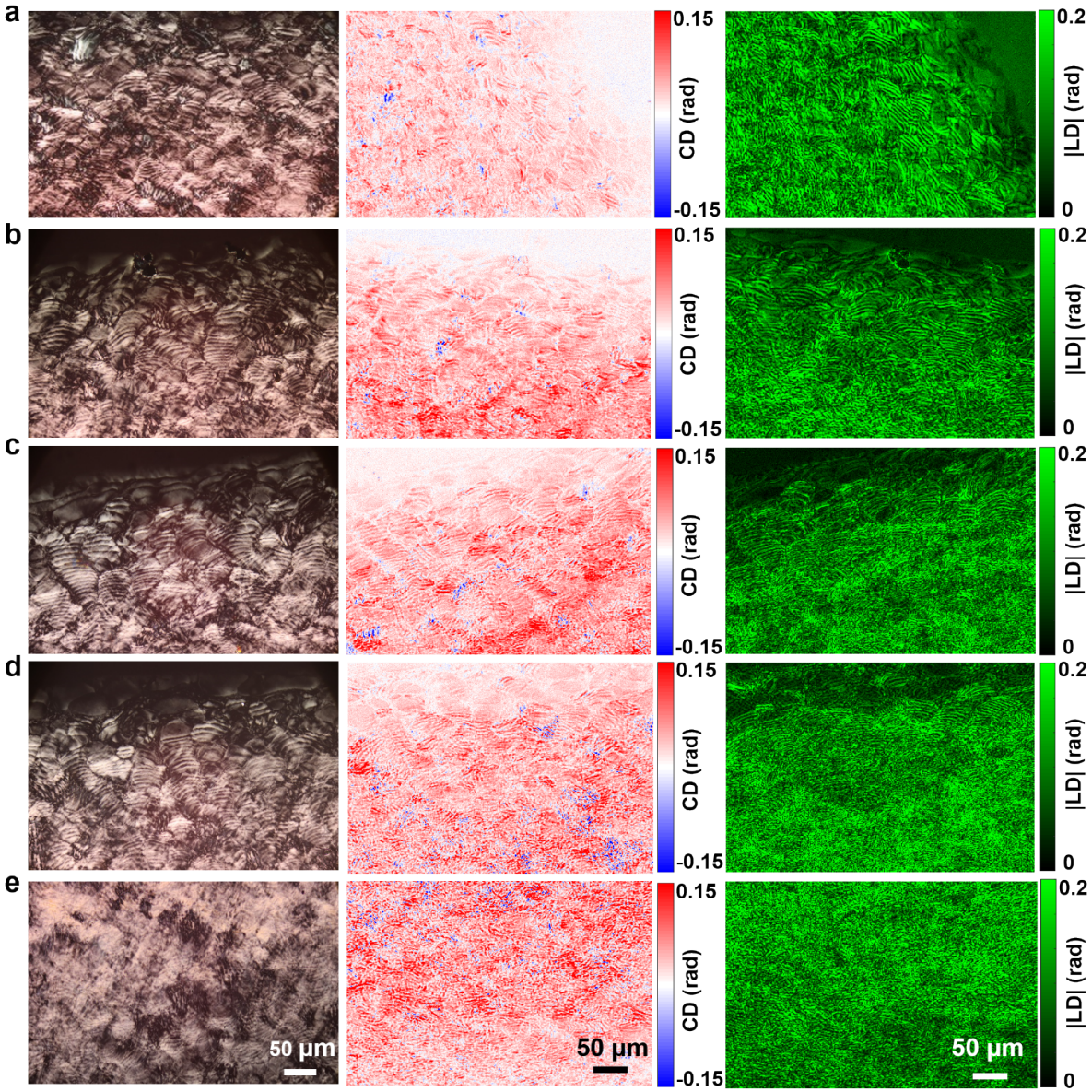

Figure S19 | Measured optical results of the CNC films with different CNCs concentrations. (a-e) C_{CNCs} = 0.50 wt.%, 1.0 wt.%, 1.5 wt.%, 2.0 wt.% and 2.5 wt.%.

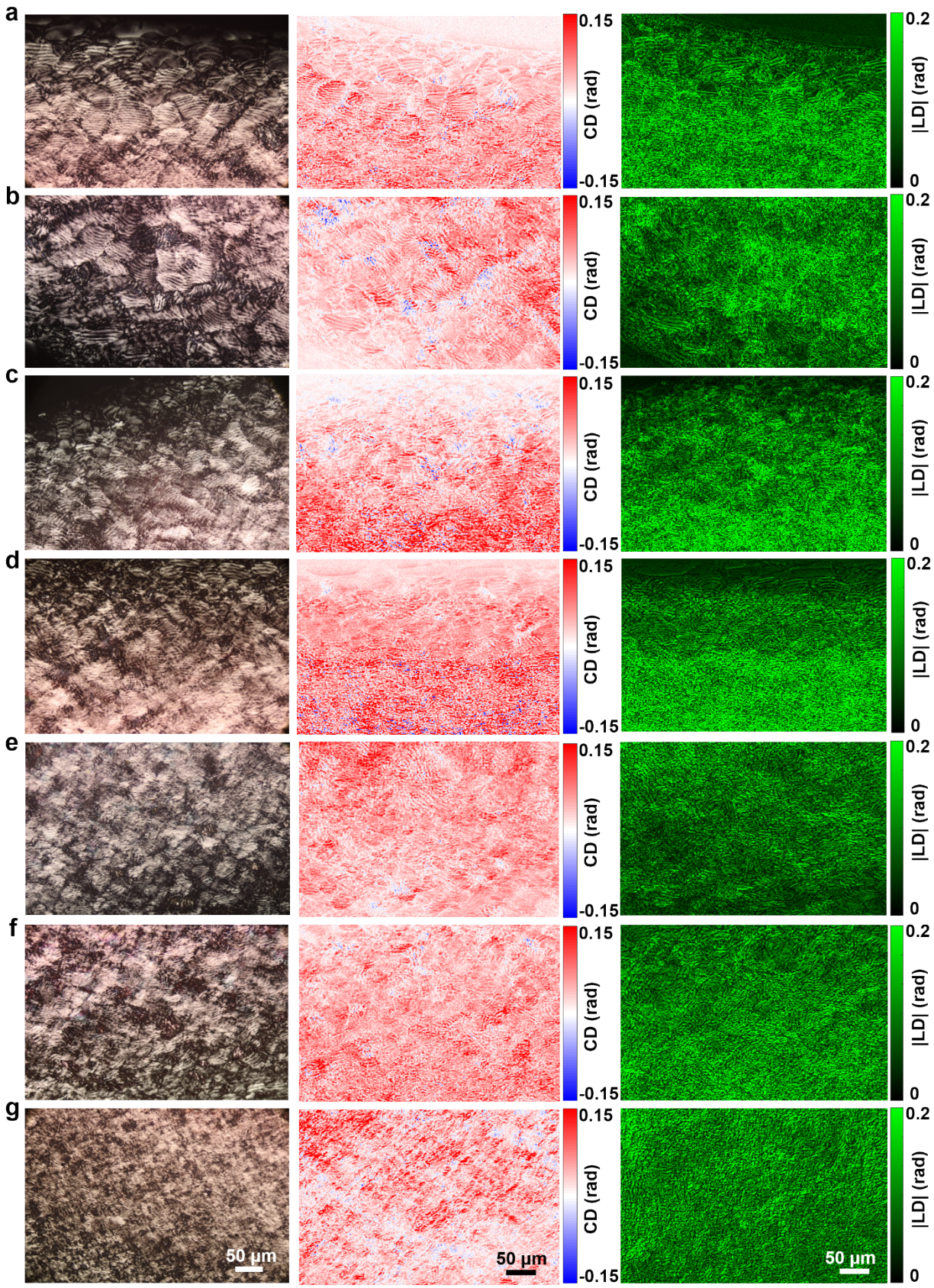

Figure S20 | Measured optical results of the CNC films with different NaCl concentrations. (a-g) C_{NaCl} = 0.0 mM, 0.20 mM, 0.50 mM, 0.75 mM, 1.0 mM, 1.3 mM and 1.5 mM.

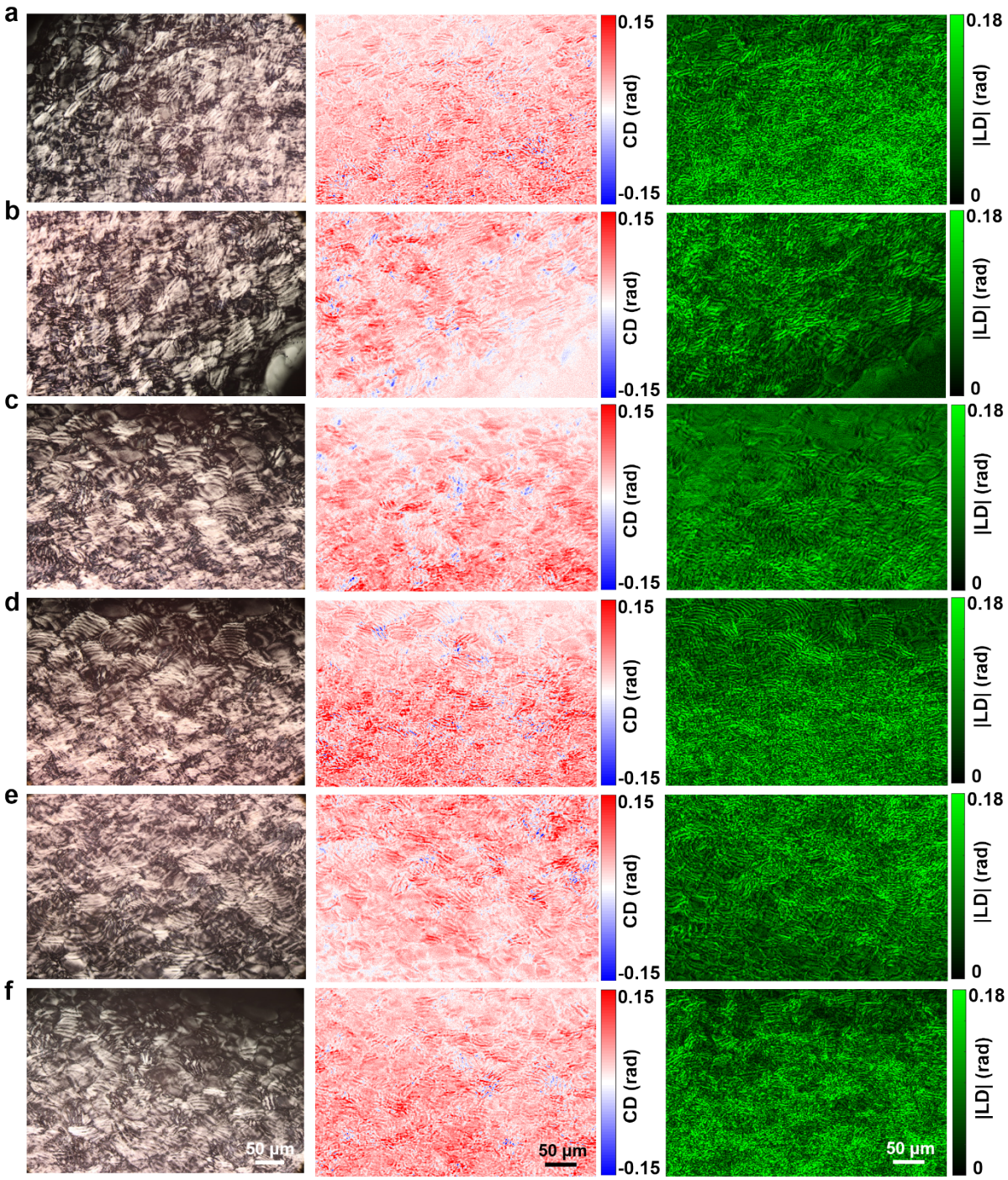

Figure S21 | Measured optical results of the CNC films with different pH. (a-f) pH = 5.1, 6.3, 7.3, 8.4, 9.5, and 10.1.

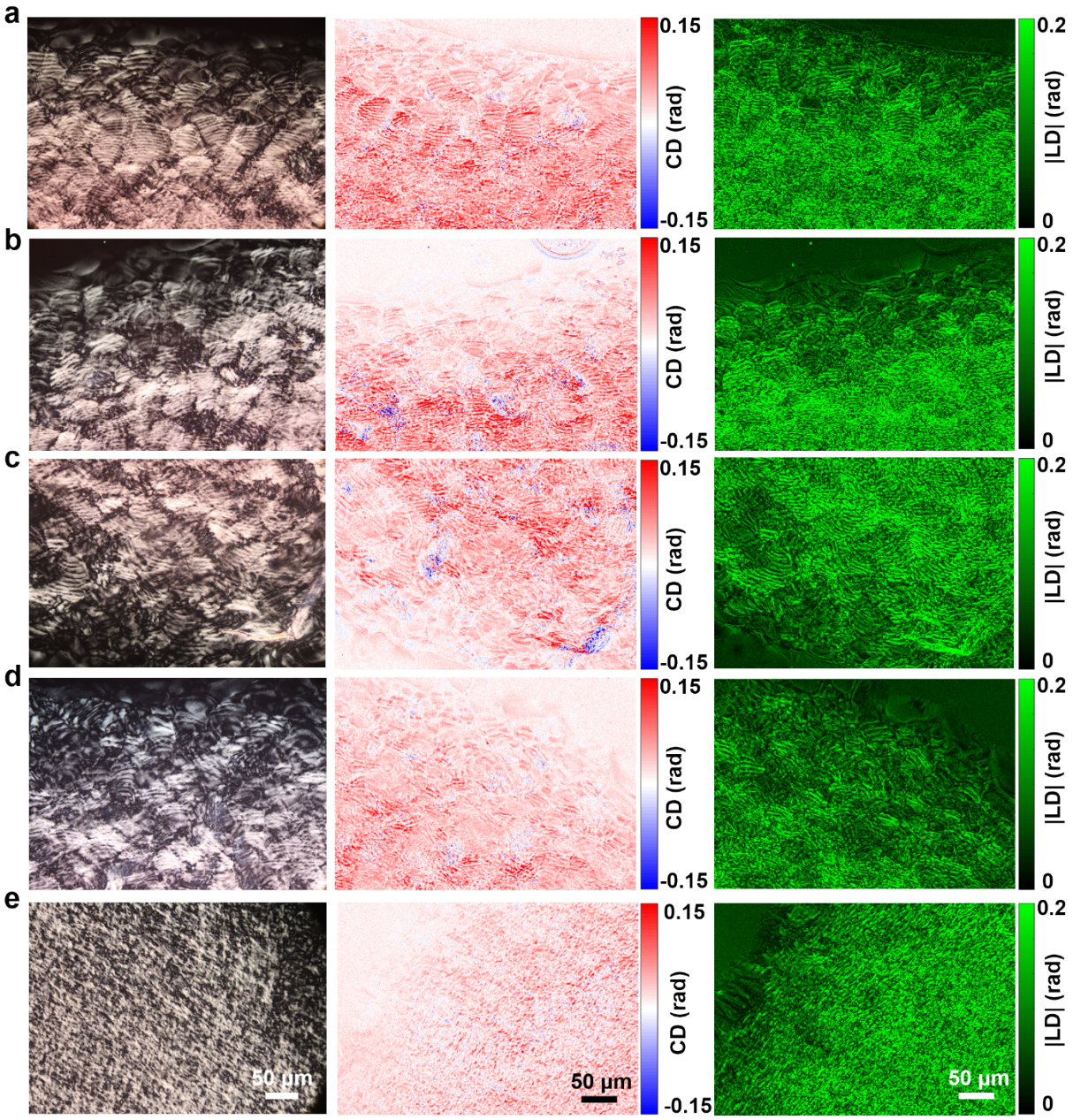

Figure S22 | Measured optical results of the CNC films formed at different temperatures. (a-e) T= 5 ˚C, 15 ˚C, 25 ˚C, 35 ˚C, and 45 ˚C.

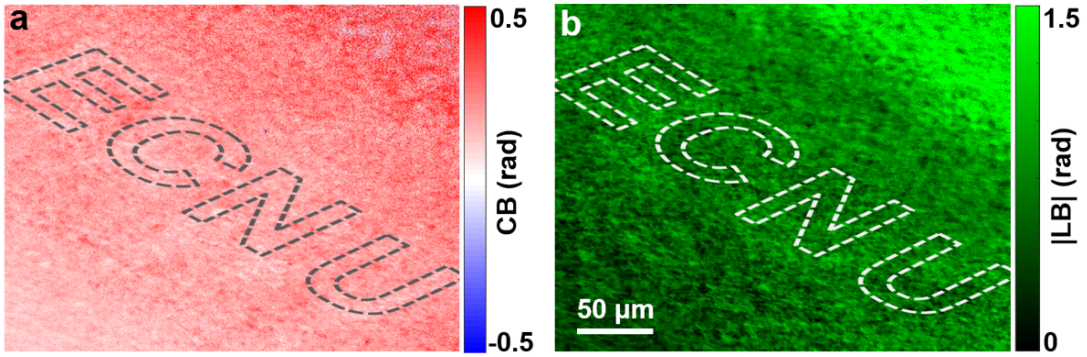

Figure S23 | The measured (a) CB and (b) |LB| images of photobleached CNC films.

4. References

1. Hauge, P. S., *J. Opt. Soc. Am.*, 1978, **68**, 1519-1528.
2. Azzam, R. M., *Opt. Lett.*, 1978, **2**, 148.
3. Goldstein, D. H., *Appl. Opt.*, 1992, **31**, 6676-6683.
4. Arteaga, O., Baldris, M., Anto, J., Canillas, A., Pascual, E., Bertran, E., *Appl. Opt.,* 2014, **53**, 2236-2245.
5. Duan, T. W., Ai, J., Cui, X. Y., Feng, X. W., Duan, Y. Y., Han, L., Jiang, J. G., Che, S. N., *Chem,* 2021, **7**, 2695-2707.
6. Dumanli, A. G., Van der Kooij, H. M., Kamita, G., Reisner, E., Baumberg, J. J., Steiner, U., Vignolini, S., *ACS Appl. Mater. Interfaces*, 2014, **6**, 12302-12306.
7. Cranston, E. D., Gray, D. G., *Colloids Surf. A Physicochem. Eng. Asp.,* 2008, **325**, 44-51.
8. Jones, R., *J. Opt. Soc. Am.,* 1942, **32**, 486-493.
9. Arteaga, O., Canillas, A., *Opt. Lett.,* 2010, **35**, 559-561.
10. Freudenthal, J., Hollis, E., Kahr, B., *Chirality,* 2009, **21**, 20-27.
11. Arteaga, O., *Opt. Lett.,* 2013, **38**, 1131-1133.
12. Stokes, G., *Trans. Cambridge Philos. Soc.,* 1852, **9**, 399.
13. Mueller, H., *Chem. Soc. Rev.,* 1948, **38**, 661.
14. Cui, X., Nichols, S. M., Arteaga, O., Freudenthal, J., Paula, F., Shtukenberg, A. G., Kahr, B., *J. Am. Chem. Soc.,* 2016, **138**, 12211-12218.